Theory of dielectric photonic crystals sandwiched between parallel metal plates

Bendtsen, Reiko Inoue; Skovsen, Esben; Søndergaard, Thomas Møller

Published in:
Optics Continuum

DOI (link to publication from Publisher):
10.1364/OPTCON.472541

Publication date:
2023

Document Version
Publisher's PDF, also known as Version of record

Citation for published version (APA):
Bendtsen, R. I., Skovsen, E., & Søndergaard, T. M. (2023). Theory of dielectric photonic crystals sandwiched between parallel metal plates. *Optics Continuum*, *2*(2), 312-326. https://doi.org/10.1364/OPTCON.472541

Research Article Vol. 2, No. 2 / 15 Feb 2023 / Optics Continuum 312

OPTICS CONTINUUM

Theory of dielectric photonic crystals sandwiched between parallel metal plates

REIKO INOUE BENDTSEN,[1] ESBEN SKOVSEN,[1] AND THOMAS MØLLER SØNDERGAARD[1,2,*]

[1] *Department of Materials and Production, Aalborg University, Skjernvej 4A, DK-9220 Aalborg øst, Denmark*
[2] *ts@mp.aau.dk*
[*] *ts@nano.aau.dk*

Abstract: Photonic crystals based on silicon-air-geometries sandwiched between parallel metal plates are studied theoretically. Compared with in-plane propagation in corresponding infinite-height photonic crystals, modes with one of the two possible polarizations are eliminated for small plate separations. Consequently, 2D photonic crystals that usually do not have a band gap for both polarizations possess a complete band gap in the sandwich geometry. A procedure for obtaining the maximum allowed photonic-crystal height between plates that preserves the in-plane band gap is described. The effect on the band gap of adding an air-gap or a silicon substrate to the photonic crystal structure between plates is also studied. Finally, it is shown that, for terahertz frequencies, a useful distance between metal plates is comparable to the thickness of thin silicon wafers, and that propagation losses are sufficiently small that the structures are of practical interest. We briefly discuss the numerical method that was used for calculating band diagrams and band gaps, which is based on a modification to the plane-wave-expansion method [R. D. Meade et. al., Phys. Rev. B **48**, 8434 (1993)] based on an iterative search algorithm exploiting Fast Fourier Transforms for fast calculations.

1. Introduction

Due to numerous technological innovations and breakthroughs in electronics, photonics, and nanotechnology made since the early 1990s, terahertz (THz) technologies have found an increasingly wide variety of applications that are more closely linked to our daily lives. The field of photonic crystals (PhCs), i.e., periodic dielectric structures in which light cannot propagate in any direction for certain frequency intervals due to the presence of a photonic band gap (PBG), was founded by Yablonovitch and John [1,2], and plays an important role in enhancing the performance, functionality, and usability of THz technologies [3–6]. For THz system integration, 2D PhC slabs with finite thickness, in particular, provide high feasibility and easiness in fabrication and are able to localize light via PBG in the plane and with index guiding in the vertical direction [7–9]. Several photonics components have been demonstrated for THz waves based on PhC slabs, such as traditional PhC-slab waveguides with low loss [10,11], cavities and resonators [12,13], diplexers (splitters) [14], dielectric antennas integrated with PhC slabs [15,16], and waveguides and sensors based on topological PhCs promising very low reflection from waveguide bends [17,18]. In all these cases the structures were based on air-holes in a silicon slab surrounded by air.

The structures of interest in this paper are different. We will focus on the properties of PhC slabs sandwiched between parallel metal plates. While metal plates may increase the propagation loss due to absorption, there are also great advantages, namely the possible elimination of one of the polarizations of light for in-plane propagation [19], and PhCs based on rods rather than holes become attractive and practical and offer large band gaps. In addition, the metal plates eliminate the possibility of out-of-plane scattering, which may especially occur from waveguide bends and

#472541 https://doi.org/10.1364/OPTCON.472541
Journal © 2023 Received 4 Aug 2022; revised 11 Jan 2023; accepted 12 Jan 2023; published 27 Jan 2023

OPTICS CONTINUUM

imperfections, and undesirable interaction via radiation with any other nearby structures is made impossible. While absorption losses are smaller for photonic-crystal slabs surrounded by air then, in our view, the losses are nevertheless small enough for THz frequencies that the use of metal plates is of practical interest for THz photonics components. The theoretical study in this paper is necessary in order to be able to design and thus realize optimum structures. Preliminary work on fabrication and characterization of PhCs between metal plates qualitatively support the theoretical results [20].

Metal parallel-plate waveguides (PPWGs) are able to confine light vertically within a narrow space between the two metal plates, and horizontally by modulating the effective refractive index [21–24]. At optical frequencies, the losses in metals are considerably large. On the other hand, similar structures have been experimentally demonstrated to exhibit low-loss transverse-magnetic (TM)-mode propagation with virtually no group velocity dispersion, for frequencies up to 4.5 THz and lengths to 0.25 m [25–30]. They also allow simulating a 3D geometry with 2D calculations since the TM mode has no spatial dependence in the direction perpendicular to the plates. Moreover, it has been shown that the lowest-order transverse-electric (TE) mode can also be utilized for THz PPWG applications with ultralow ohmic losses [31–33]. Therefore, in the past two decades, various quasioptic elements [27,28], as well as various filters, have been incorporated in such THz PPWGs in order to better control light propagation.

The majority of the research has so far been focused on metal (or metal coated dielectric) PBG structures [34–37] and PhC waveguides [23,30,38–40] as frequency filters. On the other hand, there has been very few studies on dielectric PBG structures in metal PPWGs, e.g., [41,42], which studied the optical properties with THz time-domain spectroscopy. Designing a dielectric PBG structure-filled PPWG requires taking the dielectric properties and frequency response into consideration [43], but has the advantage that dielectric PhCs are among the most thoroughly studied PhC systems [8,9], and that there is no need for a PBG for both polarizations because TE polarization waves are effectively removed by sandwiching with metal plates due to the boundary condition, in the THz range [44].

In this paper, we investigate 1D and 2D PhCs sandwiched between parallel metal plates and determine the maximum height between plates that will preserve their in-plane photonic band gap (Secs. 2 and 3). We also study how a bottom silicon layer or an upper air-gap affect the photonic band gap. This is followed by a discussion of propagation losses in the relevant parallel-metal-plate waveguides with either air or silicon (Sec. 4.), showing that propagation losses are sufficiently small in the THz frequency range. Finally, we briefly account for the plane-wave-expansion method that was used for the calculations of PhCs sandwiched between metal plates (Sec. 5.).

2. 1D-periodic PhCs in a PPWG

In this section, we consider a periodic array of silicon and air-layers (refractive indices $n_{\mathrm{Si}} = 3.42$ (applicable for THz frequencies [45]) and $n_{\mathrm{Air}} = 1$) with thicknesses $d_{\mathrm{Si}} = \Lambda n_{\mathrm{Air}}/(n_{\mathrm{Air}} + n_{\mathrm{Si}})$ and $d_{\mathrm{Air}} = \Lambda n_{\mathrm{Si}}/(n_{\mathrm{Air}} + n_{\mathrm{Si}})$, where Λ is the period. This corresponds to quarter-wave layers for the wavelength $\lambda_0 = 4\Lambda n_{\mathrm{Si}} n_{\mathrm{Air}}/(n_{\mathrm{Si}} + n_{\mathrm{Air}})$. The structure is periodic along the x-axis, and invariant along the y- and z-axes. Later in this section, we consider a finite-height of the geometry sandwiched between parallel metal plates. The reason for first considering the infinite-height geometry is that the properties of the sandwich geometry can be directly related to off-axis propagation in the infinite-height structure with discrete off-axis wave-numbers.

Due to symmetry considerations, it is sufficent for the infinite-height geometry to consider propagation only in the xy-plane. The structure supports s-polarized Bloch-modes on the form

$$\mathbf{E}(\mathbf{r}) = \hat{\mathbf{z}} U_{k_x}(x) e^{ik_x x} e^{ik_y y}, \tag{1}$$

OPTICS CONTINUUM

where $\mathbf{E}(\mathbf{r})$ is the electric field, which here is polarized along the z-axis, and $U_{k_x}(x)$ is periodic along x with the period Λ. k_x is the Bloch-wave number, and k_y is the off-axis-propagation wave number. The magnetic-field is polarized in the xy-plane. A time-factor of $\exp(-i\omega t)$ is implicit (free-space wave-number $k_0 = \omega/c$, where c is the vacuum speed of light). The structure also supports p-polarized modes on the same form except that the magnetic field $\mathbf{H}(\mathbf{r})$ is polarized along the z-axis, and the electric field is in the xy-plane. The dispersion relations of propagating modes can be found by solving [46,47]

$$\cos(k_x\Lambda) = \cos(k_{x,\mathrm{Air}}d_{\mathrm{Air}})\cos(k_{x,\mathrm{Si}}d_{\mathrm{Si}}) - \frac{1}{2}\left(P + \frac{1}{P}\right)\sin(k_{x,\mathrm{Air}}d_{\mathrm{Air}})\sin(k_{x,\mathrm{Si}}d_{\mathrm{Si}}), \tag{2}$$

where $P = k_{x,\mathrm{Air}}/k_{x,\mathrm{Si}}$ for s-polarization, and $P = \varepsilon_{\mathrm{Si}}k_{x,\mathrm{Air}}/\varepsilon_{\mathrm{Air}}k_{x,\mathrm{Si}}$ for p-polarization, and $k_{x,\mathrm{u}} = \sqrt{k_0^2\varepsilon_u - k_y^2}$, and the dielectric constants $\varepsilon_u = n_u^2$, where subscript u represents either air or silicon. Propagating modes exist whenever the magnitude of the right-hand side of Eq. (2) does not exceed 1.

A projected band structure showing the propagating modes versus k_0 and k_y for both polarizations is shown in Fig. 1. The geometry is seen to have a large in-plane band gap ($k_y = 0$), but no complete band gap. In addition, it is seen that, if $k_y\Lambda/2\pi > 1.09$ (corresponds to the vertical dashed line in Fig. 1), all propagating modes are pushed to higher frequencies than the in-plane band gap.

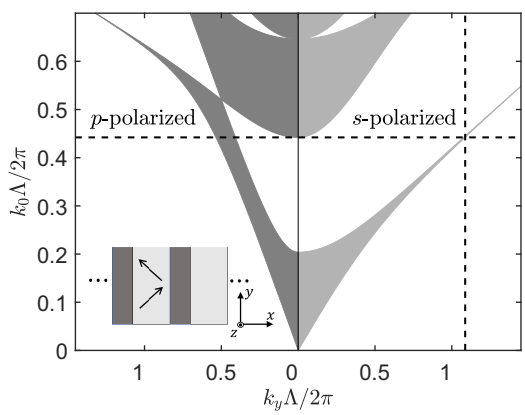

Fig. 1. Projected band structure for a one-dimensional PhC of quarter-wave silicon and air layers (for details see text). The minimum required off-axis wave-number (vertical dashed line) that pushes frequencies of all propagating modes above the band gap of on-axis propagation is identified.

Now consider a finite-height H (along y) of the same PhC sandwiched between perfect conductors (Fig. 2). The result in Fig. 2 was obtained by solving Eq. (2) using discrete values of k_y. In this case, p- and s-polarized modes behave as $\cos(k_y y)$ or $\sin(k_y y)$, respectively, along the y-axis between the plates with $k_y = m\pi/H$, where $m = 0, 1, 2, \ldots$. In-plane propagating modes ($m = 0$) for s-polarization thus vanishes. The out-of-plane propagating modes ($m>0$) are equivalent to those considered in Fig. 1. The modes propagate up and down between the metal plates along the y-axis, and only discrete values of k_y satisfy the electromagnetics boundary conditions at the metal interfaces. The maximum allowed height $H = 0.46\Lambda$ that preserves the band gap is now found by setting the limit found from Fig. 1, i.e. $k_y = 1.09 \cdot 2\pi/\Lambda$, equal to $k_y = \pi/H$.

The solid black lines in Fig. 2 correspond to $k_y = 0$. These bands exist for all chosen H. For $H = 0.46\Lambda$, additional bands exist, where one of them just touches the upper limit of the band

OPTICS CONTINUUM

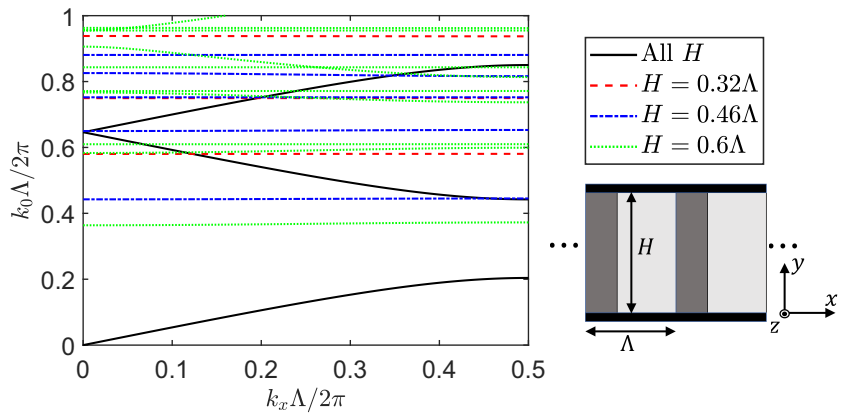

Fig. 2. Band structure for a finite height H of the one-dimensionally periodic PhC considered in Fig. 1 sandwiched between metal plates. Three heights, $H = 0.32\Lambda$, 0.46Λ, and 0.6Λ, are considered.

gap. A higher $H = 0.6\Lambda$ is seen to lead to a new band inside the in-plane band gap, while a smaller $H = 0.32\Lambda$ removes the additional bands further from the band gap. Notice that the additional bands are very narrow in frequency, which agrees with Fig. 1.

The main conclusion from this analysis is that, if $H<0.46\Lambda$, the band structure for the sandwich structure is identical to the band structure of the infinite-height PhC for on-axis propagation (propagation along the x-axis) up to and including the band gap. Thus, a sufficiently small H preserves the band gap known from normal incidence.

It may be of practical interest to fabricate a finite-height 1D-periodic PhC by etching into a silicon wafer, but without etching all the way through the silicon. In this way, the silicon regions are supported by a bottom silicon layer of thickness b (see inset in left part of Fig. 3). The geometry can then easily and practically be surrounded by an upper and lower metal plate. Alternatively, it may also happen that the upper metal plate cannot be placed directly on top of the silicon due to fabrication imperfections, which may lead to an air-gap of thickness g above the structure (see inset in the right part of Fig. 3). The upper and lower edge of the band gap is shown in Fig. 3 versus b and g for different choices of the height between metal plates H.

In Figs. 1 and 2, we considered a simpler geometry with layers of either air or silicon, which is simpler to model. Here, it is also possible, in the limit of a very small H, to consider similar layers, but with an effective dielectric constant based on effective-medium theory [48]. For the case of an air layer of thickness $H - b$ above a silicon substrate of thickness b, the effective dielectric constant in the limit of very small H is given by [48]

$$\frac{1}{\varepsilon_{\text{eff}}} = \frac{b}{H}\frac{1}{\varepsilon_{Si}} + \left(1 - \frac{b}{H}\right)\frac{1}{\varepsilon_{air}}. \tag{3}$$

A calculation based on the effective-medium theory is also shown in Fig. 3. The band-edges are seen to converge to the effective-medium limit as H decreases. It is interesting to observe in Eq. (3) that a bottom silicon layer of a small thickness b does not change the effective dielectric constant a lot since ε_{Si} is more than 10 times larger than $\varepsilon_{air} = 1$. In the other case with an air-gap g, the effective dielectric constant is instead given by

$$\frac{1}{\varepsilon_{\text{eff}}} = \frac{g}{H}\frac{1}{\varepsilon_{air}} + \left(1 - \frac{g}{H}\right)\frac{1}{\varepsilon_{Si}}. \tag{4}$$

The effect of a finite g will thus, for the same reason, have a significant impact on the effective dielectric constant. It is seen from Fig. 3 that a sizable b and g can be maintained without losing

OPTICS CONTINUUM

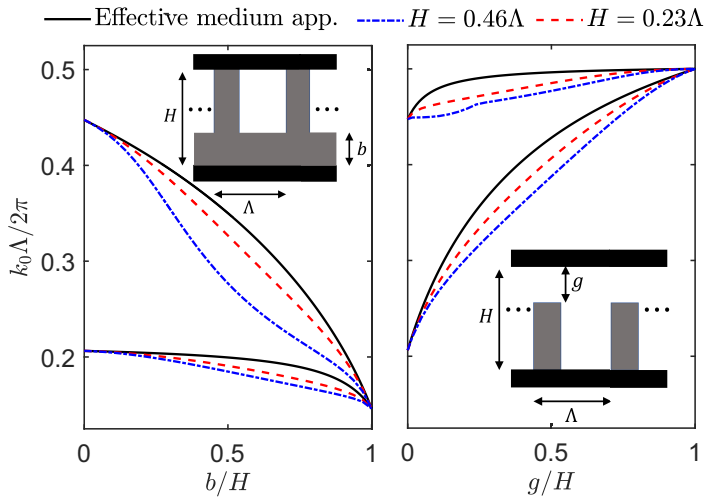

Fig. 3. Band gap for a finite height of the PhC considered in Fig. 1 when adding a silicon substrate of thickness b or an air-gap of thickness g.

the band gap. The results in Fig. 3 were obtained by using the plane-wave expansion method with a perfect conductor boundary condition applied at $y = 0$ and $y = H$ (Sec. 5.). The result in Fig. 2 was also confirmed by using this method.

3. 2D-periodic PhCs in a PPWG

In this section, we consider two-dimensionally periodic PhCs of a finite height sandwiched between parallel metal plates. Such structures have previously been modeled in Ref. [19]. Similar to the 1D case, the properties of the sandwich geometry are directly related to out-of-plane propagation modes with discrete wave-numbers of the infinite-height PhC. Therefore, we first consider a periodic array of infinite-height silicon rods arranged on a square lattice. The geometry is periodic in the xy-plane and invariant along the z-axis. The radius of silicon rods is $a = 0.2\Lambda$, where Λ is the period (see inset in Fig. 4). The Bloch-modes are thus on the form

$$\mathbf{E}(\mathbf{r}) = \mathbf{U}_{k_x,k_y}(x, y)e^{ik_x x}e^{ik_y y}e^{ik_z z}. \tag{5}$$

The band structure for in-plane propagation ($k_z = 0$) in this geometry (Fig. 4) shows that there is a large band gap for TM-polarization and no band gap for TE-polarization. The latter polarization corresponds to having the electric field polarized in the xy-plane following the definition in [8]. When sandwiching a small finite height H of this geometry between parallel metal plates, the TE-polarized modes will be eliminated (due to the boundary conditions at the metal surfaces), leaving a structure with a quite large complete band gap.

The projected band structure showing the existence of guided modes versus k_z and k_0 is presented in Fig. 5. This diagram was made by fixing k_z and calculating band structures similar to Fig. 4, and then repeating that for each k_z. In this procedure, we include modes with any polarization. As can be seen from Fig. 5, there is no (complete) in-plane band gap. However, the in-plane band gap for TM polarization is marked in the figure. It is seen that if $k_z\Lambda/2\pi > 0.526$ (right vertical line in Fig. 5), all bands are pushed above the upper edge of the in-plane TM band gap.

Now consider the sandwich geometry where parallel metal plates are inserted at $z = 0$ and $z = H$. The modes found in Fig. 5 may in principle propagate up and down between the metal plates, but boundary conditions must be met at the metal surfaces. Some field components will

OPTICS CONTINUUM

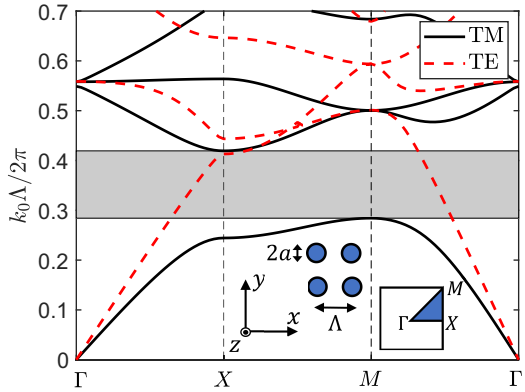

Fig. 4. Band structure for in-plane propagation in a periodic array of infinite-height silicon rods with radius $a = 0.2\Lambda$ on a square lattice. Modes with two polarizations exist (TE and TM). A band gap only exists for TM polarization.

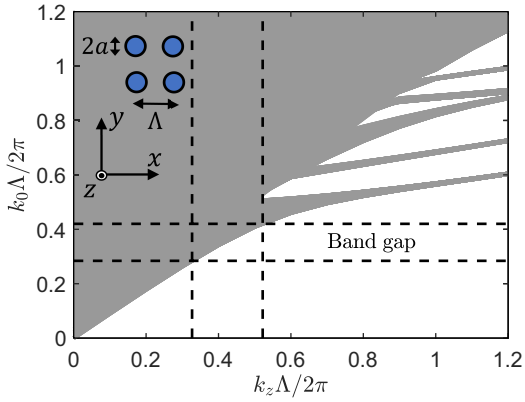

Fig. 5. Projected band structure for the PhC considered in Fig. 4. The band gap edges for TM-polarization from Fig. 4 are marked with horizontal dashed lines. Out-of-plane wave-numbers that push all bands either above the bottom or top edges of the band gap are shown with vertical dashed lines.

thus behave as $\sin(k_z z)$ and others as $\cos(k_z z)$, where we have to require that $k_z = m\pi/H$ (similar to the 1D case). In the case of $m = 0$, the boundary conditions eliminate the TE polarized modes. If we now use $\pi/H = 0.526 \cdot 2\pi/\Lambda$, we find $H = 0.95\Lambda$. The band structure for the sandwich geometry with this height is shown in the left part of Fig. 6. Notice that the TM bands from Fig. 4 are also found here, whereas the TE bands are absent. There are additional bands for frequencies above the in-plane TM band gap just touching the upper edge of the band gap. There is thus no difference compared with the in-plane TM-band-structure for frequencies up to and including the in-plane TM band gap. If we again consider Fig. 5, we notice that $k_z\Lambda/2\pi = 0.327$ (left vertical dashed line) only pushes bands to the lower edge of the in-plane TM band gap. This k_z is equivalent to using $H = 1.53\Lambda$. However, as an example, we choose H in the middle of the two extremes, i.e. $H = 1.24\Lambda$, and show the band structure for that case in the right half of Fig. 6. Notice that the additional bands now extend into the region of the in-plane TM band gap, thus effectively reducing the band gap to approximately half of the original size. The main conclusion from this example is that although the 2D PhC as such does not possess a complete in-plane band

OPTICS CONTINUUM

gap, the corresponding sandwich geometry does just that if the height H is sufficiently small (H<0.95Λ).

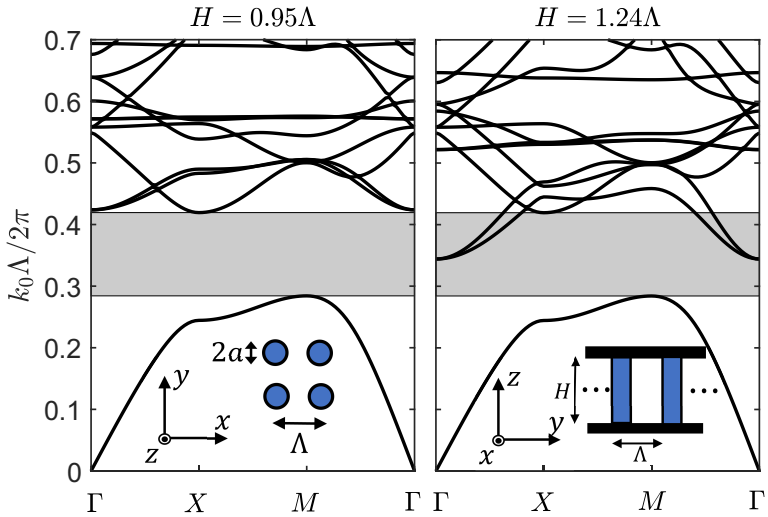

Fig. 6. Band structure for a 2D periodic array of silicon rods of finite height H sandwiched between parallel metal plates. At $H = 0.95\Lambda$ additional bands just touch the upper limit of the in-plane propagation band gap, while $H = 1.24\Lambda$ effectively reduces the band gap to half-size.

If we now wish to apply this geometry for a frequency of 0.5 THz (wavelength $\lambda_0 = 600\ \mu$m), considering the normalized frequency 0.35 (approximately in the center of the band gap), then the period must be $\Lambda = 0.35\lambda_0 = 210\ \mu$m. The requirement of H<0.95Λ then means that we must require $H \leq 200\ \mu$m, matching a standard thin silicon wafer thickness.

It may be practical to fabricate rods by lithography and subsequent etching of a silicon wafer, in which case it is convenient to keep a bottom silicon layer for stability. Also, when sandwiching the PhC between metal plates an air-gap between the rods and the upper metal film may, e.g., occur as a consequence of thickness variations of the silicon wafer. The effect on the band gap of a bottom silicon layer of thickness b, or an air-gap of thickness g, is studied in Fig. 7 for a few different total distances H between the two metal films.

We can use the effective-medium expressions (3) and (4) in the limit of a very small H , and effectively reduce the 3D problem to a 2D problem. In this limit the band gap is seen to exist for quite large values of b/H exceeding 50%, which is a result of a layer with high dielectric constant only having a small effect, as is clear from Eq. (3). In the case of 1D PhCs (Sec. 2.) any contrast between low- and high-refractive index regions would produce a bandgap, and therefore the band gap existed for any b/H<1. Here, a finite contrast is needed, and thus the maximum allowed b/H that produces a band gap is smaller. As the spacing H increases, the maximum allowed b/H that produces a band gap is seen to decrease, which can be understood in the way that light can better localize in the high-refractive-index material for large H, which leads to a larger effective dielectric constant than the limit given in Eq. (3). The contrast is thus effectively reduced as H increases. Also note that the band-gap edges decrease in frequency with increasing b as expected when increasing the amount of high-refractive-index material [8].

In the case of the air-gap it is seen in the effective-medium limit (very small H) that the band gap disappears for g/H exceeding app. 0.2 in accordance with an air-gap having a large effect on the effective dielectric constant as seen from Eq. (4). It is interesting that as H increases the band gap exists for larger values of g/H. Again, this can be explained as a consequence of light being

OPTICS CONTINUUM

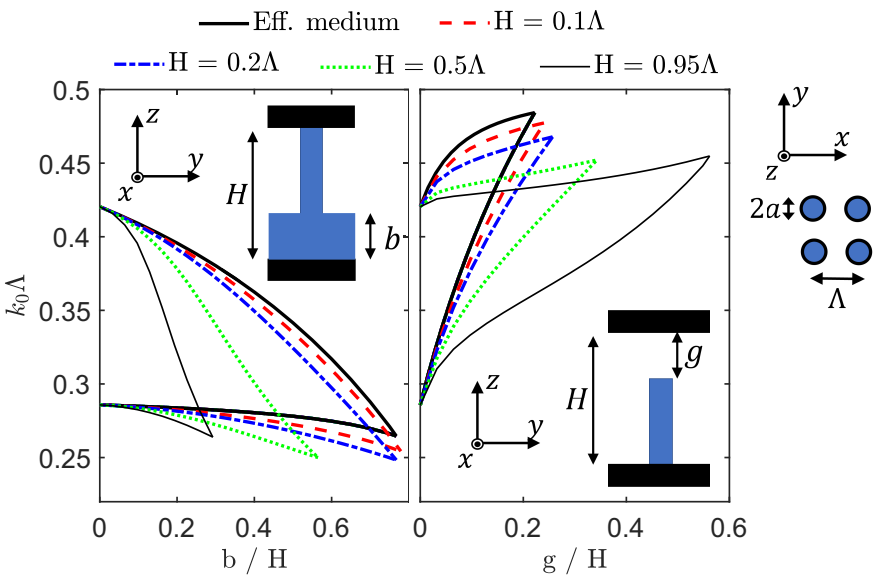

Fig. 7. Band gap for a periodic array of silicon rods on a rectangular lattice placed between parallel metal plates versus either a bottom silicon layer of thickness b between the bottom metal plate and the rods, or an air-gap of thickness g between the silicon rods and the upper metal plate. Calculations are shown for a couple of different total distances between the metal plates.

able to better localize in the high-refractive-index material as H increases, which to some extent reduces the effect of the air gap. Limits such as $H = 0.95\Lambda$, band diagrams similar to Fig. 6, and studies such as the one in Fig. 7, have not been shown previously in related work [19].

We will consider one more typical 2D PhC, namely an array of air-holes in silicon arranged on a hexagonal lattice (see inset in Fig. 8). Again, we consider first this geometry as being periodic in the xy-plane and invariant along the z-axis. The expression in Eq. (5) also applies here. The projected band structure for this geometry with air-holes of radius $r = 0.48\Lambda$, where Λ is the distance between the center of neighbor air-holes, is shown in Fig. 8. A complete in-plane band gap ($k_z = 0$) is clearly identified in the figure. It is well-known that for sufficiently large air-holes, this type of geometry supports a complete in-plane PBG [8]. It is observed that if $k_z\Lambda/2\pi>0.862$, all bands are pushed to higher frequencies than the upper edge of the in-plane band gap. Comparing this with $k_z = \pi/H$, we find $H = 0.58\Lambda$. In a similar way, we find that $H = 0.72\Lambda$ will push additional bands to frequencies matching the lower band-gap-edge or higher. We will use the average value $H = 0.65\Lambda$ that should effectively reduce the in-plane band gap to half-size. This is exactly what is observed in Fig. 9, which shows the band structures for the sandwich geometry for $H = 0.58\Lambda$ and $H = 0.65\Lambda$, respectively, in the left and right parts of the figure. In the case of $H = 0.58\Lambda$, the in-plane band gap is preserved, whereas a higher H leads to additional bands entering the in-plane band gap region, reducing its size.

Considering again the frequency of 0.5 THz and now a normalized frequency of 0.5 (approximately in the center of the band gap), the period must be $\Lambda = 0.5\lambda_0 = 300\ \mu$m. The requirement of $H<0.58\Lambda$ then means that we must require $H<174\ \mu$m. In that case, we are well on the safe side of securing the band gap by using a standard thin-silicon-wafer thickness of, e.g., 100-150 μm, which are commercially available.

OPTICS CONTINUUM

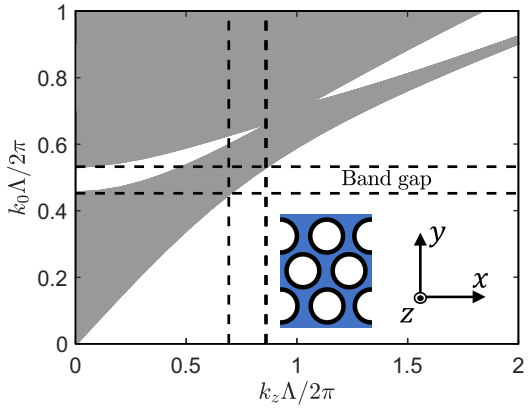

Fig. 8. Projected band structure for a PhC with air-holes of radius $r = 0.48\Lambda$ placed on a hexagonal lattice in silicon. A complete in-plane band gap exists. Out-of-plane wave numbers corresponding to out-of-plane propagating modes at the upper and lower limits of the in-plane band gap are identified (vertical dashed lines).

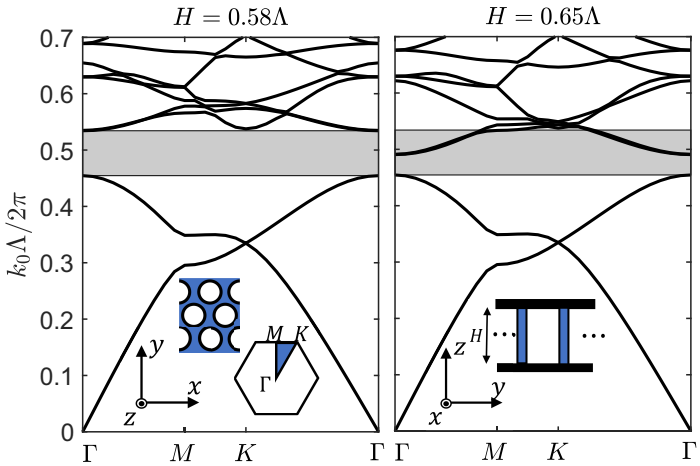

Fig. 9. Band structure for a 2D periodic array of holes on a hexagonal lattice in a silicon slab of finite height H sandwiched between parallel metal plates. At $H = 0.58\Lambda$ additional bands just touch the upper limit of the in-plane-propagation band gap, while $H = 0.65\Lambda$ effectively reduces the band gap to half-size.

For completeness, we show in Fig. 10 how the band gap is affected by a bottom silicon layer, or a top air-gap, between the PhC slab and one of the metal films The overall trends are similar to those found for the array of rods on a square lattice in Fig. 7.

The results in this section were all obtained using the plane-wave-expansion method that we discuss in Sec. 5.

OPTICS CONTINUUM

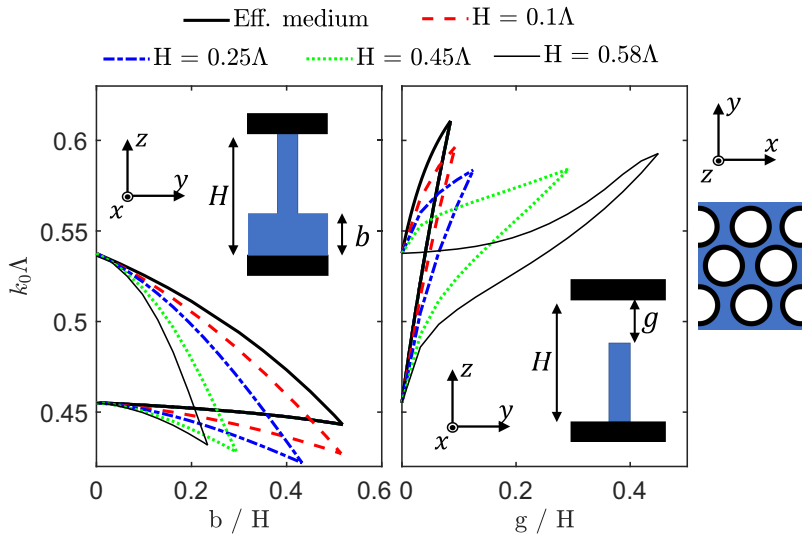

Fig. 10. Band gap for a periodic array of holes on a hexagonal lattice in a silicon slab sandwiched between parallel metal plates versus either a bottom silicon layer of thickness b between the lower metal plate and the slab, or an air-gap of thickness g between the slab and the upper metal film. The total distance between metal plates is H. Band gaps are shown for a few different total thicknesses H versus b/H or g/H.

4. Mode-index of parallel-plate aluminium waveguide with air or silicon

In this section, we address the question of propagation loss in a parallel-metal-plate waveguide with either silicon or air between the plates using aluminium for the metal. We consider a fixed frequency of 0.5 THz, which is equivalent to a wavelength of $\lambda_0 = 600\mu$m. The modes in such a geometry have, e.g., an electric field on the form

$$\mathbf{E}(\mathbf{r}) = \mathbf{E}_0(z)e^{ik_x x}. \tag{6}$$

We define $n_\mathrm{m} = n_r + in_i \equiv k_x/k_0$ as the mode-index. The dispersion of guided modes, and thus the mode-index, can be found by solving the equation

$$1 - \left(r^{(p)}_{\mathrm{d,m}}(k_x)\right)^2 e^{2ik_{z,d}H} = 0, \tag{7}$$

where $r^{(p)}_{\mathrm{d,m}}(k_x)$ is the Fresnel reflection coefficient for p-polarization at the metal-dielectric interface, and $k_{z,d} = \sqrt{k_0^2\varepsilon_d - k_x^2}$, where subscript d represents either air or silicon. We consider only p-polarization since a fundamental guided mode exists for this polarization when $H<\lambda_0/2n_d$, where $n_d = \sqrt{\varepsilon_d}$ is the refractive index of the dielectric between the plates. The s-polarized modes exist only for $H>\lambda_0/2n_d$, where higher-order p-polarized modes also appear.

A detailed description of how to solve Eq. (7) numerically by searching in the complex plane can be found in appendix F in [49]. We apply the complex refractive index $n_\mathrm{Al} = 709.68 + i752.26$ for aluminium [50] and $n_\mathrm{Si} = 3.42 + i0.0002$ for silicon [45]. In this way, absorption losses in both aluminium and silicon are included. Taking into account the very small imaginary part of of the silicon refractive index, on the other hand, is not particularly important.

In the case of the waveguide with air between the aluminium plates (Fig. 11(a)), there is only one solution at 0.5 THz for $H<300$ μm with a real part of the mode-index of approx. 1 and an imaginary part easily smaller than 0.001. At $H = 100$ μm, we find $n_i = 0.00063$, which is

OPTICS CONTINUUM

equivalent to a propagation length of $L = \lambda_0/(2\pi n_i) = 15$ cm, and if using $H = 200$ μm, the propagation length is approx. twice as large.

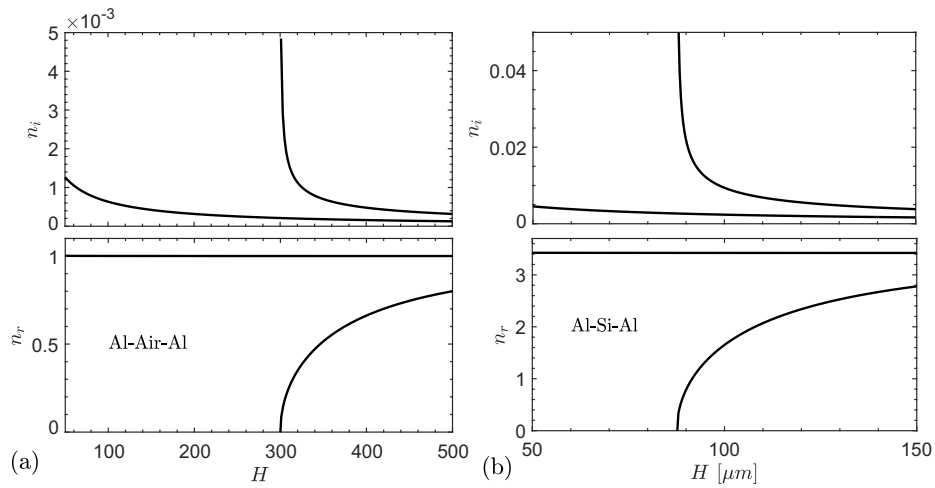

Fig. 11. Real (n_r) and imaginary (n_i) parts of the mode index for p-polarized modes in a parallel-plate waveguide with (a) air, or (b) silicon, sandwiched between aluminium surfaces versus air or silicon layer thickness H for a fixed frequency of 0.5 THz.

In the case of the waveguide with silicon between the aluminium plates (Fig. 11(b)), there is only one solution for H<300 μm/n_{Si} = 87.7μm. Considering here the fundamental mode at $H = 100$ μm, we find $n_i = 0.0024$, leading to the propagation length of 4 cm. These propagation lengths are sufficiently large compared with the wavelength and corresponding periods of PhCs that PhCs sandwiched between metal plates at THz frequencies are of practical interest, e.g., for integrated THz photonics.

5. Plane-wave-expansion method

The band diagrams in this paper have been calculated by solving the magnetic-field wave equation

$$\nabla \times \frac{1}{\varepsilon(\mathbf{r})} \nabla \times \mathbf{H}(\mathbf{r}) = k_0^2 \mathbf{H}(\mathbf{r}), \tag{8}$$

by using a plane-wave (Fourier) expansion of the magnetic field $\mathbf{H}(\mathbf{r})$, and solving the wave equation as an eigenvalue problem using an iterative approach. The program used for the calculations is an in-house matlab implementation of the method described in [51], which one of the authors (TS) also applied for photonic-crystal waveguide slabs a couple of decades ago [52,53] (back then in a Fortran implementation). Here, we will briefly review the method, and explain how it has been adapted to handle confinement between parallel metal plates.

In Eq. (8), $\varepsilon(\mathbf{r})$ is the periodic dielectric constant, and $k_0 = \omega/c$ is the free-space wave-number. The wave equation thus represents an eigenvalue problem, where k_0^2 is the eigenvalue. The dielectric constant is periodic in the xy-plane. In the case where the PhC is confined between parallel metal plates at $z = 0$ and $z = H$, it is convenient to handle the boundary conditions at the metal surfaces by considering a fully periodic structure in all three dimensions with period $2H$ along the z-axis, where the range $0 \leq z \leq H$ contains the structure of interest. The structure being used in the calculation, however, does not have any metal plates but is mirror symmetric around the plane $z = H$. The mirror symmetry thus defines the structure in the region $H \leq z \leq 2H$. For a symmetric structure the solutions can be divided into even and odd solutions (depending on field

OPTICS CONTINUUM

component), and we simply restrict the solution space to the symmetry with vanishing x- and y-components of the electric field at $z = 0$ and $z = H$, i.e., when we solve Eq. (8) iteratively, we only search for solutions that satisfy the appropriate symmetry. This approach has the advantage that it only requires a slight modification to the well-known plane-wave-expansion approach for modeling of periodic dielectric structures using an iterative approach [51,54].

The magnetic field is assumed to be a Bloch-wave on the form

$$\mathbf{H}(\mathbf{r}) = \mathbf{U}_{\mathbf{k}}(\mathbf{r})e^{i\mathbf{k}\cdot\mathbf{r}}, \tag{9}$$

where $\mathbf{U}_{\mathbf{k}}(\mathbf{r})$ is a periodic function with the same period as the dielectric constant. Thus, $\varepsilon(\mathbf{r}) = \varepsilon(\mathbf{r} + \mathbf{R})$, where $\mathbf{R} = n_1\mathbf{a_1} + n_2\mathbf{a_2} + n_3\mathbf{a_3}$, where $\mathbf{a}_i$ are the lattice vectors of the periodic structure, and n_i are integers. We choose $\mathbf{a}_1$ and $\mathbf{a}_2$ to be in the xy-plane, while $\mathbf{a}_3 = \hat{\mathbf{z}}2H$ is the period along the z-axis.

The magnetic field is expressed as

$$\mathbf{H}(\mathbf{r}) = \sum_{\mathbf{G},\sigma} H_{\mathbf{G},\sigma}\hat{\mathbf{h}}_{\mathbf{G},\sigma}e^{i(\mathbf{G}+\mathbf{k})\cdot\mathbf{r}}, \tag{10}$$

where the index $\sigma = 1, 2$ represents two magnetic-field directions being perpendicular to $\mathbf{G} + \mathbf{k}$, i.e.

$$\hat{\mathbf{h}}_{\mathbf{G},1} = \frac{\hat{\mathbf{z}} \times (\mathbf{G} + \mathbf{k})}{|\hat{\mathbf{z}} \times (\mathbf{G} + \mathbf{k})|}, \quad \text{and} \quad \hat{\mathbf{h}}_{\mathbf{G},2} = \frac{\mathbf{G} + \mathbf{k}}{|\mathbf{G} + \mathbf{k}|} \times \hat{\mathbf{h}}_{\mathbf{G},1}. \tag{11}$$

This ensures that $\nabla \cdot \mathbf{H}(\mathbf{r}) = 0$.

The reciprocal lattice vectors $\mathbf{G}$ are given by

$$\mathbf{G} = n_1\mathbf{b}_1 + n_2\mathbf{b}_2 + n_3\mathbf{b}_3, \tag{12}$$

where n_1, n_2 and n_3 are integers, and the elementary reciprocal lattice vectors $\mathbf{b}_i$ satisfy $\mathbf{a}_i \cdot \mathbf{b}_j = 2\pi\delta_{i,j}$.

By choosing $\mathbf{k}$, and inserting (10) into the wave Eq. (8), and then solving the wave equation, we find frequencies k_0 corresponding to each $\mathbf{k}$. Thus, by sweeping $\mathbf{k}$ over the edge of the irreducible Brillouin zone, we obtain the band diagrams.

It is exploited that the operator $\Theta = \nabla \times \frac{1}{\varepsilon(\mathbf{r})}\nabla\times$ is Hermitian for positive and real dielectric constants [8], since in that case we can find eigensolutions iteratively by modifying $\mathbf{H}(\mathbf{r})$ via the Fourier coefficients such that the energy functional

$$E(\mathbf{H}(\mathbf{r})) = \frac{\langle\mathbf{H}(\mathbf{r})|\Theta|\mathbf{H}(\mathbf{r})\rangle}{\langle\mathbf{H}(\mathbf{r})|\mathbf{H}(\mathbf{r})\rangle} \tag{13}$$

is minimized. The overlap integrals are defined by an integral over the unit cell

$$\langle\mathbf{H}_1(\mathbf{r})|\mathbf{H}_2(\mathbf{r})\rangle = \int_{\text{u.c.}} (\mathbf{H}_1(\mathbf{r}))^* \cdot \mathbf{H}_2(\mathbf{r})d^d r, \tag{14}$$

where * represents complex conjugation, and d is the dimensionality of the problem. The overlap integrals can be straightforwardly expressed using a sum over Fourier coefficients [54].

The iterative approach is similar to the one presented in Ref. [55], and it is very efficient, since carrying out the rotations $\nabla\times$ requires only one operation for each plane wave in (10) when the magnetic field is represented in reciprocal space (by the Fourier coefficients $H_{\mathbf{G},\sigma}$), while the division by $\varepsilon(\mathbf{r})$ is carried out by first Fourier-transforming $\nabla \times \mathbf{H}(\mathbf{r})$ from reciprocal space to real-space using the Fast Fourier Transform, in which case $\nabla \times \mathbf{H}(\mathbf{r})$ is known on discrete points, and division by ε now requires only one operation for every point in real space. The result is then Fourier-transformed back to reciprocal space, in which case the last rotation $\nabla\times$ can be carried

OPTICS CONTINUUM

out with one operation for every plane wave. Convergence is drastically improved by a tensor representation of ε based on different averaging for electric fields parallel and perpendicular to interfaces [51]. The method uses very little memory, and carrying out the operator Θ scales as $N \log N$, where N is the number of plane waves. In order to keep the number of required iterations small a preconditioned conjugate gradient algorithm is applied [55], in which small spatial frequencies are given higher weight.

The modification that we have made to this method in order to handle confinement between metal plates is that, first of all, we choose $\mathbf{k} = \hat{\mathbf{x}}k_x + \hat{\mathbf{y}}k_y + \hat{\mathbf{z}}k_z$ to have $k_z = 0$, and then we search for the solutions that satisfy

$$H_{n_1\mathbf{b}_1+n_2\mathbf{b}_2+n_3\mathbf{b}_3,\sigma=1} = H_{n_1\mathbf{b}_1+n_2\mathbf{b}_2-n_3\mathbf{b}_3,\sigma=1}, \tag{15}$$

$$H_{n_1\mathbf{b}_1+n_2\mathbf{b}_2+n_3\mathbf{b}_3,\sigma=2} = -H_{n_1\mathbf{b}_1+n_2\mathbf{b}_2-n_3\mathbf{b}_3,\sigma=2}. \tag{16}$$

This straightforwardly leads to the solutions with vanishing x- and y-components of the electric field at $z = 0$ and $z = H$ as required. The sum of terms with $n_3 = \pm m$ leads to behaviour as either $\sin(mz\pi/H)$ or $\cos(mz\pi/H)$. In Ref. [19] the *electric field* was expanded from the start in terms behaving in this way, and solutions for PhCs were found using a standard matrix eigenvalue-problem approach (not an iterative method). Apart from the metal plates no variation in the dielectric constant along z was considered in Ref. [19].

In the case of a 2D periodic structure as considered in, e.g., Fig. 5 (structure being invariant along z) we use

$$\mathbf{G} = n_1\mathbf{b}_1 + n_2\mathbf{b}_2, \tag{17}$$

and control the out-of-plane propagation using k_z. While we do not in this paper model a PhC slab surrounded by air then this can also be done by repeating slabs along z with a large separation (super-cell approach), and in that case with no restrictions on $H_{\mathbf{G},\sigma}$.

6. Conclusion

We have presented the principles of determining the maximum allowed height of a PhC layer sandwiched between parallel metal plates that will preserve the in-plane TM-polarization band gap of the 2D PhC. For the 2D PhC, the out-of-plane propagation wave-number that pushes all bands above the in-plane band gap was matched to the first higher-order discrete out-of-plane wave-number of the sandwich geometry, which leads to a restriction on the height. Using a larger height than the limit effectively reduces the band gap, while a smaller height preserves the band gap. This principle was demonstrated for both 1D and 2D PhCs: for quarter-wave layers of Si and Air in the 1D case and for both silicon rods on a square lattice and holes in silicon on a hexagonal lattice in the 2D case. We also studied how a spacer between the PhC and metal plates in the form of an air-gap or silicon substrate will reduce the band gap. According to effective-medium theory the silicon substrate is expected to have a smaller effect on the band gap than the air-gap, and this was indeed found to be the case for small distances between the metal plates. However, with increasing distances between plates, the better possibility of localization of electromagnetic waves in the high-refractive-index medium meant that air-gaps had a smaller effect, such that a quite large relative air-gap could be tolerated, while the tolerable relative thickness of the silicon substrate was reduced.

We furthermore found that, for a frequency of 0.5 THz and aluminium for the metal, we can use PhCs based on wafer thicknesses of 100 μm or 200 μm, depending on the specific geometry, and propagation lengths in parallel-plate waveguides with air or silicon (approx. 15 cm, or 4 cm, respectively, for a thickness of 100 μm) are sufficiently large that the geometries considered are of practical interest.

Acknowledgments. The authors acknowledge Anders M. Westerkam, Jesper L. W. Sonne, and Karl G. Danielsen, for helpful discussions [20].

OPTICS CONTINUUM

Disclosures. The authors declare no conflicts of interest.

Data availability. Data underlying the results presented in this paper are available upon request from the corresponding author.

References

1. E. Yablonovitch, "Inhibited spontaneous emission in solid-state physics and electronics," Phys. Rev. Lett. **58**(20), 2059–2062 (1987).
2. S. John, "Strong localization of photons in certain disordered dielectric superlattices," Phys. Rev. Lett. **58**(23), 2486–2489 (1987).
3. M. Tonouchi, "Cutting-edge terahertz technology," Nat. Photonics **1**(2), 97–105 (2007).
4. J.-S. Rieh, *Introduction to Terahertz Electronics* (Springer Nature Switzerland AG, 2021), 1st ed.
5. T. Nagatsuma, "Terahertz technologies: present and future," IEICE Electron. Express **8**(14), 1127–1142 (2011).
6. E. Linfield, "A source of fresh hope," Nat. Photonics **1**(5), 257–258 (2007).
7. M. Fujita, S. Takahashi, Y. Tanaka, T. Asano, and S. Noda, "Simultaneous inhibition and redistribution of spontaneous light emission in photonic crystals," Science **308**(5726), 1296–1298 (2005).
8. J. D. Joannopoulos, S. G. Johnson, J. N. Winn, and R. D. Meade, *Photonic Crystals: Molding the Flow of Light* (Princeton University Press, 2018), 2nd ed.
9. S. G. Johnson, S. Fan, P. R. Villeneuve, J. D. Joannopoulos, and L. A. Kolodziejski, "Guided modes in photonic crystal slabs," Phys. Rev. B **60**(8), 5751–5758 (1999).
10. K. Tsuruda, M. Fujita, and T. Nagatsuma, "Extremely low-loss terahertz waveguide based on silicon photonic-crystal slab," Opt. Express **23**(25), 31977–31990 (2015).
11. D. Headland, M. Fujita, and T. Nagatsuma, "Bragg-mirror suppression for enhanced bandwidth in terahertz photonic crystal waveguides," IEEE J. Select. Topics Quantum Electron. **26**(2), 1–9 (2020).
12. S. M. Hanham, C. Watts, W. J. Otter, S. Lucyszyn, and N. Klein, "Dielectric measurements of nanoliter liquids with a photonic crystal resonator at terahertz frequencies," Appl. Phys. Lett. **107**(3), 032903 (2015).
13. S. M. Hanham, M. M. Ahmad, S. Lucyszyn, and N. Klein, "Led-switchable high-q packaged thz microbeam resonators," IEEE Trans. THz Sci. Technol. **7**(2), 199–208 (2017).
14. M. Yata, M. Fujita, and T. Nagatsuma, "Photonic-crystal diplexers for terahertz-wave applications," Opt. Express **24**(7), 7835–7849 (2016).
15. W. Withayachumnankul, R. Yamada, M. Fujita, and T. Nagatsuma, "All-dielectric rod antenna array for terahertz communications," APL Photonics **3**(5), 051707 (2018).
16. D. Headland, W. Withayachumnankul, R. Yamada, M. Fujita, and T. Nagatsuma, "Terahertz multi-beam antenna using photonic crystal waveguide and luneburg lens," APL Photonics **3**(12), 126105 (2018).
17. A. Kumar, M. Gupta, P. Pitchappa, Y. J. Tan, N. Wang, and R. Singh, "Topological sensor on a silicon chip," Appl. Phys. Lett. **121**(1), 011101 (2022).
18. Y. Yang, Y. Yamagami, X. Yu, P. Pitchappa, J. Webber, B. Zhang, M. Fujita, T. Nagatsuma, and R. Singh, "Terahertz topological photonics for on-chip communication," Nat. Photonics **14**(7), 446–451 (2020).
19. A. A. Maradudin and A. R. McGurn, "Photonic band structure of a truncated, two-dimensional, periodic dielectric medium," J. Opt. Soc. Am. B **10**(2), 307–313 (1993).
20. K. G. Grundahl, J. L. W. Sonne, and A. M. Westerkam, *Terahertz photonics utilizing photonic crystals exhibiting Fano resonances and photonic band gaps (Master thesis)* (Aalborg University, 2022).
21. K. Tanaka and M. Tanaka, "Simulations of nanometric optical circuits based on surface plasmon polariton gap waveguide," Appl. Phys. Lett. **82**(8), 1158–1160 (2003).
22. F. Kusunoki, T. Yotsuya, J. Takahara, and T. Kobayashi, "Propagation properties of guided waves in index-guided two-dimensional optical waveguides," Appl. Phys. Lett. **86**(21), 211101 (2005).
23. B. Wang and G. P. Wang, "Confining light in two-dimensional slab photonic crystal waveguides with metal plates," Appl. Phys. Lett. **88**(19), 193128 (2006).
24. B. Wang and G. P. Wang, "Plasmon Bragg reflectors and nanocavities on flat metallic surfaces," Appl. Phys. Lett. **87**(1), 013107 (2005).
25. D. R. Grischkowsky, "Optoelectronic characterization of transmission lines and waveguides by terahertz time-domain spectroscopy," IEEE J. Select. Topics Quantum Electron. **6**(6), 1122–1135 (2000).
26. R. Mendis and D. Grischkowsky, "Undistorted guided-wave propagation of subpicosecond terahertz pulses," Opt. Lett. **26**(11), 846–848 (2001).
27. S. Coleman and D. Grischkowsky, "A THz transverse electromagnetic mode two-dimensional interconnect layer incorporating quasi-optics," Appl. Phys. Lett. **83**(18), 3656–3658 (2003).
28. J. Dai, S. Coleman, and D. Grischkowsky, "Planar THz quasioptics," Appl. Phys. Lett. **85**(6), 884–886 (2004).
29. Y. Zhao and D. Grischkowsky, "Terahertz demonstrations of effectively two-dimensional photonic bandgap structures," Opt. Lett. **31**(10), 1534–1536 (2006).
30. Y. Zhao and D. R. Grischkowsky, "2-D terahertz metallic photonic crystals in parallel-plate waveguides," IEEE Trans. Microwave Theory Techn. **55**(4), 656–663 (2007).
31. R. Mendis and D. M. Mittleman, "Multifaceted terahertz applications of parallel-plate waveguide: TE1 mode," Electron. Lett. **46**(26), S40–S44 (2010).

OPTICS CONTINUUM

32. M. Mbonye, R. Mendis, and D. M. Mittleman, "Inhibiting the TE1-mode diffraction losses in terahertz parallel-plate waveguides using concave plates," Opt. Express **20**(25), 27800–27809 (2012).
33. R. Mendis and D. M. Mittleman, "An investigation of the lowest-order transverse-electric (te1) mode of the parallel-plate waveguide for THz pulse propagation," J. Opt. Soc. Am. B **26**(9), A6–A13 (2009).
34. A. Bingham, Y. Zhao, and D. Grischkowsky, "THz parallel plate photonic waveguides," Appl. Phys. Lett. **87**(5), 051101 (2005).
35. J. Kitagawa, M. Kodama, S. Koya, Y. Nishifuji, D. Armand, and Y. Kadoya, "THz wave propagation in two-dimensional metallic photonic crystal with mechanically tunable photonic-bands," Opt. Express **20**(16), 17271–17280 (2012).
36. J. Kitagawa, M. Kodama, Y. Nishifuji, D. Armand, and Y. Kadoya, "New design of terahertz metallic photonic crystal with mechanically tunable photonic-band-gap," in *Proceedings of the International Quantum Electronics Conference and Conference on Lasers and Electro-Optics Pacific Rim 2011*, (Optica Publishing Group, 2011), paper C233 (2011).
37. S. Wang, W. Lu, X. Chen, Z. Li, X. Shen, and W. Wen, "Two-dimensional photonic crystal at THz frequencies constructed by metal-coated cylinders," J. Appl. Phys. **93**(11), 9401–9403 (2003).
38. A. L. Bingham and D. R. Grischkowsky, "Terahertz 2-d photonic crystal waveguides," IEEE Microw. Wireless Compon. Lett. **18**(7), 428–430 (2008).
39. D. Armand, S. Koya, and Y. Kadoya, "Photonic crystal sandwiched in parallel plates as THz waveguide," *2013 38th International Conference on Infrared, Millimeter, and Terahertz Waves (IRMMW-THz)* pp. 1–2 (2013).
40. H. Li, M. X. Low, R. T. Ako, M. Bhaskaran, S. Sriram, W. Withayachumnankul, B. T. Kuhlmey, and S. Atakaramians, "Compact terahertz photonic crystal chip sandwiched in parallel metallic plates," arXiv, arXiv: Opt. (2019).
41. Z. Jian, J. Pearce, and D. M. Mittleman, "Two-dimensional photonic crystal slabs in parallel-plate metal waveguides studied with terahertz time-domain spectroscopy," Semicond. Sci. Technol. **20**(7), S300–S306 (2005).
42. H. Li, M. X. Low, R. T. Ako, M. Bhaskaran, S. Sriam, W. Withayachumnankul, B. T. Kulmey, and S. Atakaramians, "Broadband single-mode hybrid photonic crystal waveguides for terahertz integration on a chip," Adv. Mater. Technol. **5**(7), 2000117 (2020).
43. C. P. Yuan and T. H. Chang, "Modal analysis of metal-stub photonic band gap structures in a parallel-plate waveguide," Prog. Electromagn. Res. **119**, 345–361 (2011).
44. D. J. Griffiths, *Introduction to Electrodynamics* (Cambridge University Press, 2017), 4th ed.
45. J. Dai, J. Zhang, W. Zhang, and D. Grischkowsky, "Terahertz time-domain spectroscopy characterization of the far-infrared absorption and index of refraction of high-resistivity, float-zone silicon," J. Opt. Soc. Am. B **21**(7), 1379–1386 (2004).
46. L. Novotny and B. Hecht, *Principles of Nano-Optics* (Cambridge University Press, 2012), 2nd ed.
47. M. Skorobogatiy and J. Yang, *Fundamentals of Photonic Crystal Guiding* (Cambridge University Press, 2009).
48. W. Cai and V. Shalaev, *Optical metamaterials* (Springer, 2010).
49. T. M. Søndergaard, *Green's Function Integral Equation Methods in Nano-Optics* (CRC Press, 2019).
50. H.-J. Hagemann, W. Gudat, and C. Kunz, "Optical constants from the far infrared to the x-ray region: Mg, Al, Cu, Ag, Au, Bi, C, and Al_2O_3," J. Opt. Soc. Am. **65**(6), 742–744 (1975).
51. R. D. Meade, A. M. Rappe, K. D. Brommer, J. D. Joannopoulos, and O. L. Alerhad, "Accurate theoretical analysis of photonic band-gap materials," Phys. Rev. B **48**(11), 8434–8437 (1993).
52. T. Søndergaard and A. Lavrinenko, "Large-bandwidth planar photonic crystal waveguides," Opt. Commun. **203**(3-6), 263–270 (2002).
53. T. Søndergaard, J. Arentoft, and M. Kristensen, "Theoretical analysis of finite-height semiconductor-on-insulator-based planar photonic crystal waveguides," J. Lightwave Technol. **20**(8), 1619–1626 (2002).
54. S. G. Johnson and J. D. Joannopoulos, "Block-iterative frequency-domain methods for maxwell's equations in a planewave basis," Opt. Express **8**(3), 173–190 (2001).
55. M. P. Teter, M. C. Payne, and D. C. Allan, "Solution of schrödinger's equation for large systems," Phys. Rev. B **40**(18), 12255–12263 (1989).